

Optimal Transmit Power and Flying Location for UAV Covert Wireless Communications

Shihao Yan, *Member, IEEE*, Stephen V. Hanly, *Fellow, IEEE*, and Iain B. Collings, *Fellow, IEEE*

Abstract—This paper jointly optimizes the flying location and wireless communication transmit power for an unmanned aerial vehicle (UAV) conducting covert operations. This is motivated by application scenarios such as military ground surveillance from airborne platforms, where it is vital for a UAV’s signal transmission to be undetectable by those within the surveillance region. Specifically, we maximize the communication quality to a legitimate ground receiver outside the surveillance region, subject to: a covertness constraint, a maximum transmit power constraint, and a physical location constraint determined by the required surveillance quality. We provide an explicit solution to the optimization problem for one of the most practical constraint combinations. For other constraint combinations, we determine feasible regions for flight, that can then be searched to establish the UAV’s optimal location. In many cases, the 2-dimensional optimal location is achieved by a 1-dimensional search. We discuss two heuristic approaches to UAV placement, and show that in some cases they are able to achieve close to optimal, but that in other cases significant gains can be achieved by employing our developed solutions.

Index Terms—Covert communication, UAV networks, transmit power allocation, location optimization.

I. INTRODUCTION

As a wide range of applications of Unmanned Aerial Vehicle (UAV) networks are emerging (e.g., military surveillance, forest fire detection, vehicle traffic control), ever more demanding requirements are being placed on their communication systems [2, 3]. Recent advances have included an optimization framework of user scheduling and association, power control, and trajectory design [4], as well as altitude optimisation for UAV communication platforms aiming to maximise radio coverage on the ground [5]. Practical issues, including user location uncertainty, wind speed uncertainty, and polygonal no-fly zones have been considered in optimizing the resource allocation and trajectory for multiuser UAV communications [6]. The fundamental rate limits have been explored for UAV-enabled multiple access channels, where multiple ground users transmit individual information to a mobile UAV and where the UAV’s trajectory is optimized to maximize the average sum-rate of all the users [7].

In this paper we consider UAV applications that require covert communications. We are motivated by application scenarios such as military ground surveillance from airborne platforms, where it is vital for a UAV’s signal transmission to be undetectable by those within the surveillance region.

Specifically, we focus on the problem of jointly optimizing the UAV’s location and transmit signal power to maximize the communication quality to a legitimate ground receiver outside the surveillance region, subject to: a covertness constraint, a maximum transmit power constraint, and a physical location constraint determined by the required surveillance quality.

Secure communications have been considered for UAV networks in non-covert applications, including the possibility of enhancing physical layer security (e.g., [8–14]). In [8] a UAV-enabled mobile relay was proposed to improve physical layer security, where the UAV served as a mobile relay and optimized its location in order to enhance wireless communication security. In [9] it was shown that a UAV can increase the achieved secrecy rate with an optimal flight trajectory, by simultaneously improving the channel quality to a legitimate receiver while reducing the channel quality to an eavesdropper. In [11] a UAV was used as an external jammer to transmit artificial noise, aiming to prevent an eavesdropper from eavesdropping on confidential information, where the joint optimization of the UAV’s trajectory and transmit power was considered. A similar application scenario was also investigated in [10, 12, 14], where the secrecy outage probability, jamming coverage, and joint trajectory were considered in order to show the effectiveness of using a UAV-jammer to enhance physical layer security. None of these papers addressed covertness of communications.

To operate a UAV in a surveillance scenario, it is necessary to shield the very existence of its wireless transmissions, used for conveying surveillance results back to ground stations. Covert communication technology focuses on hiding the wireless transmission from a legitimate transmitter, commonly called Alice, to an intended receiver, Bob, in the presence of a warden Willie, who is trying to detect this covert transmission [15–17]. The fundamental limit of covert communication was established in [18], which was extended into different scenarios by considering various constraints and practical issues, including noise uncertainty [19], uninformed jammer [20], relay networks [21, 22], generative adversarial networks [23], full-duplex technique [24, 25], and multiple antennas [26, 27].

Most recently, covert communication has been considered for UAV networks. In [28], a UAV’s trajectory and transmit power were jointly optimized in order to aid it transmitting critical information to a legitimate ground user without being detected by Willie. In [29] the UAV was acting as the warden Willie and a multi-hop relaying strategy (e.g., the number of hops, transmit power) was optimized to maximize the throughput of a ground network subject to a covertness constraint. The horizontal trajectory (with a fixed height) of a

S. Yan, S. V. Hanly, and I. B. Collings are with the School of Engineering, Macquarie University, Sydney, NSW, Australia (Emails: {shihao.yan, stephen.hanly, iain.collings}@mq.edu.au).

Part of this work has been presented in IEEE ICC 2019 [1].

UAV was tackled in [28], where multiple ideal assumptions, e.g., infinite symbols in each flying time slot and line-of-sight (LoS) channels, were adopted.

In this work, we address the covertness of UAV wireless transmission in a scenario where the UAV conducts surveillance over a specific area and has to urgently transmit critical information back to a legitimate user covertly. We assume that Willie is in the surveillance area and the UAV flies in the vertical plane determined by the locations of Bob and Willie. We tackle the joint optimization of the UAV's location (distance and angle relative to Willie) and transmit power in order to maximize the communication quality at Bob subject to: 1) a covertness constraint (i.e., the total error rate at Willie is no less than a specific value), 2) a maximum transmit power constraint at the UAV, 3) a lower bound on the UAV's angle to Willie, and 4) a lower bound and an upper bound on the UAV's distance to Willie. The lower bound on the distance is to prevent the UAV getting too close to Willie where it could be observed. The lower bound on the angle is to ensure that the UAV gets a good enough view of the surveillance area near Willie, and the upper bound on the distance is to ensure sufficient image resolution.

Our main contributions are as follows:

- We identify six scenarios that can arise due to the possible parameter and constraint combinations, and in each scenario provide expressions that significantly reduce the feasible region search space in order to find the UAV's optimal location.
- We explicitly show that in some scenarios, the UAV's 2-dimensional optimal location can be achieved by a 1-dimensional search.
- In the scenario where the distance between Bob and Willie is large relative to the lower and upper bounds on the UAV's distance to Willie, the most common scenario in practice, we explicitly determine the UAV's optimal location and transmit power. We show that the UAV's nearest feasible location to Bob (which naturally provides the strongest signal to Bob when not blocked) is not always the optimal location for covert communications.
- In the special case where the UAV is constrained to only fly directly above the surveillance area we solve the optimization problem explicitly. We show that the achieved effective signal-to-noise ratio (SNR) at Bob increases with the upper limit on the UAV's height.

The remainder of this paper is organized as follows: Section II details our considered system model with the adopted assumptions, Section III considers the 2-dimensional location for the UAV, where six different scenarios are examined, in Section IV we consider the vertical UAV case, and numerical results are presented in Section V. In Section VI we draw conclusions.

II. SYSTEM MODEL

A. Channel Model

The scenario of interest for covert communications in the context of UAV networks is illustrated in Fig. 1, where each of the UAV (i.e., Alice), Bob, and Willie is equipped

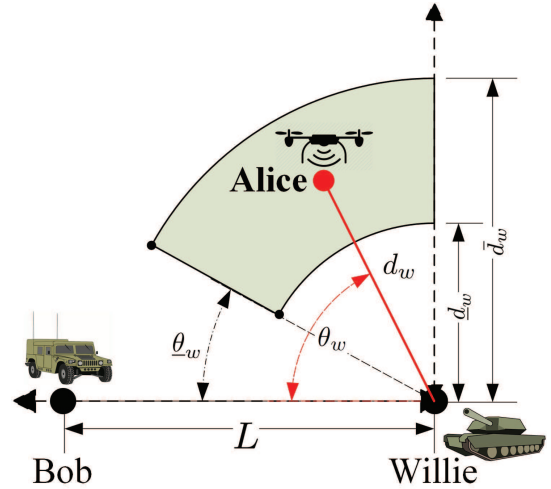


Fig. 1. Illustration of the system model for delay-constrained covert communications with UAV.

with a single antenna. In this scenario, the UAV tries to transmit critical information to Bob covertly, while Willie is trying to detect this covert transmission to determine the presence of the UAV. Specifically, Alice transmits n symbols $x[i]$ ($i = 1, 2, \dots, n$) to Bob, while Willie is collecting the corresponding observations on Alice's transmission to detect whether or not a wireless transmission took place. In this work, we consider a practical scenario, where the transmission from Alice to Bob is subject to a delay constraint (the UAV collects some urgent information on the surveillance object and has to transmit this information in a timely manner to Bob), i.e., the transmitted signals are constrained by a maximum blocklength n . We denote the additive white Gaussian noise (AWGN) at Bob and Willie as $\omega_b[i]$ and $\omega_w[i]$, respectively, where $\omega_b[i] \sim \mathcal{N}(0, \sigma_b^2)$ and $\omega_w[i] \sim \mathcal{N}(0, \sigma_w^2)$, while σ_b^2 and σ_w^2 are the noise variances at Bob and Willie, respectively. In addition, we assume that $x[i]$, $\omega_b[i]$, and $\omega_w[i]$ are mutually independent. The transmit power of the UAV is denoted as P , i.e., we have $\mathbb{E}\{|x[i]|^2\} = P$. We also consider a maximum transmit power constraint $P \leq P_m$, where P_m is the UAV's maximum transmit power.

The channels from the UAV to Bob and Willie are modelled as air-to-ground wireless channels with non-line-of-sight (NLoS) and probabilistic LoS components. Specifically, following [5] the path loss between the UAV and ground users (i.e., Bob and Willie) for the LoS and NLoS components are given by

$$\rho_j = \begin{cases} d_j^{\xi_L}, & \text{for LoS component} \\ d_j^{\xi_N}, & \text{for NLoS component,} \end{cases} \quad (1)$$

where $j \in \{b, w\}$, i.e., d_j denotes the distance from the UAV to Bob or Willie, ξ_L is the path loss exponent for the LoS channel component, and ξ_N is the path loss exponent for the NLoS channel component. As per [5], the LoS component does not always exist in the air-to-ground channels and the probability to have the LoS component in these channels depends on the environment parameters and the angle from

the UAV to the ground user. The considered scenario is shown in Fig. 1, where L is the distance between Bob and Willie. Considering the above specific scenario, the probability to have the LoS component in the channels from the UAV to Bob or Willie is given by

$$p_j = \frac{1}{1 + a \exp(-b[\theta_j - a])}, \quad (2)$$

where a and b are the S-curve parameters that depend on the communication environment and θ_j ($j \in \{b, w\}$) is the elevation angle (in degrees) of the UAV (Alice) relative to Bob or Willie. Following many existing works (e.g., [6, 28–30]) in the literature on UAV networks, we approximate the air-to-ground wireless channels as LoS channels with Willie's path loss given by $d_w^{\xi_L} p_w + d_w^{\xi_N}$, where $d_w^{\xi_L} p_w$ is the effective path loss for LoS components and $d_w^{\xi_N}$ is the path loss for the NLoS components. We note that we do not consider these channels as probabilistic channels, since the resultant Gaussian mixture likelihood functions lead to analytically intractable expressions for the covertness constraints.

B. Binary Hypothesis Testing at Willie

In order to detect the UAV's covert transmission, Willie has to distinguish between the following two hypotheses:

$$\begin{cases} \mathcal{H}_0 : y_w[i] = \omega_w[i], \\ \mathcal{H}_1 : y_w[i] = g x[i] + \omega_w[i], \end{cases} \quad (3)$$

where \mathcal{H}_0 denotes the null hypothesis where the UAV did not transmit signals, \mathcal{H}_1 denotes the alternative hypothesis where the UAV transmitted, $y_w[i]$ is the received signal at Willie for the i -th channel use, and g denotes the air-to-ground channel from the UAV to Willie.

In this work, we use the total error rate to measure Willie's detection performance, which is given by

$$\xi = \alpha + \beta, \quad (4)$$

where $\alpha \triangleq \Pr(\mathcal{D}_1 | \mathcal{H}_0)$ is the false positive rate, $\beta \triangleq \Pr(\mathcal{D}_0 | \mathcal{H}_1)$ is the miss detection rate, while \mathcal{D}_1 and \mathcal{D}_0 denote the binary decisions as to whether the UAV's transmission occurred or not, respectively. We note that Willie's goal is to detect the presence of the UAV's transmission with the minimum total error rate ξ^* , which is achieved by Willie's optimal detector that minimizes ξ . Then, the covertness constraint can be written as $\xi^* \geq 1 - \epsilon$, where ϵ is a small value to determine the specific required covertness [18].

The optimal test that minimizes ξ at Willie is the likelihood ratio test given by

$$\frac{\mathbb{P}_1 \triangleq \prod_{i=1}^n f(y_w[i] | \mathcal{H}_1)}{\mathbb{P}_0 \triangleq \prod_{i=1}^n f(y_w[i] | \mathcal{H}_0)} \stackrel{\mathcal{D}_1}{\geq} \stackrel{\mathcal{D}_0}{<} 1, \quad (5)$$

where $f(y_w[i] | \mathcal{H}_0)$ and $f(y_w[i] | \mathcal{H}_1)$ are the likelihood functions of $y_w[i]$ under \mathcal{H}_0 and \mathcal{H}_1 , respectively, while \mathbb{P}_0 and \mathbb{P}_1 are the likelihood function of \mathbf{y}_w under \mathcal{H}_0 and \mathcal{H}_1 , respectively. Following (3), we have

$$f(y_w[i] | \mathcal{H}_0) = \mathcal{N}(0, \sigma_w^2). \quad (6)$$

In this work, considering that the path loss of the NLoS component is much larger than that of the LoS component in a channel, under \mathcal{H}_1 we approximate the channel from Alice to Willie effectively as LOS and thus following (3) we have

$$f(y_w[i] | \mathcal{H}_1) = \mathcal{N}(0, \bar{P} + \sigma_w^2), \quad (7)$$

where $\bar{P} = P d_w^{\xi_L} p_w + P d_w^{\xi_N}$ is the effective received power at Willie if the UAV's wireless transmission is taking place. The optimal test at Willie can be constructed as per (5), based on which the detection performance at Willie in terms of the minimum total error rate can be derived [31]. However, we note that incomplete gamma functions are involved in the expression for the minimum total error rate [31], which is difficult in further analysis. As such, in the following we present a lower bound on this minimum total error rate in terms of the KL divergence, which is given by [18, 32]

$$\xi^* \geq 1 - \sqrt{\frac{1}{2} \mathcal{D}_{01}}, \quad (8)$$

where \mathcal{D}_{01} is the KL divergence from \mathbb{P}_0 to \mathbb{P}_1 given by

$$\mathcal{D}_{01} = \frac{n}{2} \left[\ln \left(\frac{\bar{P} + \sigma_w^2}{\sigma_w^2} \right) - \frac{\bar{P}}{\bar{P} + \sigma_w^2} \right]. \quad (9)$$

We note that the KL divergence from \mathbb{P}_1 to \mathbb{P}_0 can also be used to achieve another lower bound on ξ . However, as shown in [32] the lower bound based on \mathcal{D}_{01} is tighter in our considered system model. As such, following (8) we employ the following covertness constraint in this work

$$\mathcal{D}_{01} \leq 2\epsilon^2, \quad (10)$$

as it is sufficient to ensure $\xi^* \geq 1 - \epsilon$. Therefore, in the remaining part of this work we use $\mathcal{D}_{01} \leq 2\epsilon^2$ as the covertness constraint.

C. Delay-Constrained Transmission from the UAV to Bob

The received signal at Bob for each channel use is

$$y_b[i] = h x[i] + \omega_b[i], \quad (11)$$

where h is the air-to-ground channel from the UAV to Bob. Following [5] and considering that the path loss for NLoS component in the air-to-ground channel is much larger than that of the LoS component, in this work we approximate the SNR at Bob effectively as

$$\gamma_b(P, d_w, \theta_w) = \frac{P d_b^{\xi_L} p_b}{\sigma_b^2} = \frac{P f(d_w, \theta_w)}{\sigma_b^2}, \quad (12)$$

where $f(d_w, \theta_w)$ is given by

$$f(d_w, \theta_w) = \frac{(L^2 + d_w^2 - 2d_w L \cos(\theta_w))^{\xi_L/2}}{1 + a \exp(-b[\frac{180}{\pi} \arcsin\left(\frac{d_w \sin(\theta_w)}{\sqrt{L^2 + d_w^2 - 2d_w L \cos(\theta_w)}}\right) - a])} \quad (13)$$

This is due to the fact that, following the geometry given in Fig. 1, we have $d_b^2 = L^2 + d_w^2 - 2d_w L \cos(\theta_w)$ and $\theta_b = \arcsin(d_w \sin(\theta_w) / \sqrt{L^2 + d_w^2 - 2d_w L \cos(\theta_w)})$. We

recall that P is the UAV's transmit power, d_b^{LoS} is the path loss from the UAV to Bob, and p_b is the probability to have a LoS component in the channel from the UAV to Bob. Here, we do not consider the NLoS components in Bob's channel from the perspective of a worst-case scenario, where a lower bound on Bob's SNR can be obtained.

For a fixed transmission rate at the UAV, the decoding error probability at Bob is not negligible when n is finite and small [31]. As such, the effective throughput, which quantifies the amount of information that can be transmitted reliably from the UAV to Bob, is a reasonable performance metric for the delay-constrained communication scenarios. As proved in [33], this effective throughput is a monotonically increasing function of the corresponding SNR. As such, in this work we use the effective SNR given in (12) as the performance metric for the delay-constrained transmission from the UAV to Bob.

III. OPTIMAL LOCATION AND TRANSMIT POWER FOR A 2-DIMENSIONAL UAV

In the considered scenario, the UAV has to determine its optimal location and transmit power in order to maximize the covert communication performance. Specifically, the optimization problem at the UAV is given by

$$\operatorname{argmax}_{P, d_w, \theta_w} \gamma_b(P, d_w, \theta_w), \quad (14a)$$

$$\text{s.t. } \mathcal{D}_{01} \leq 2\epsilon^2, \quad (14b)$$

$$P \leq P_m, \quad (14c)$$

$$\underline{d}_w \leq d_w \leq \bar{d}_w, \quad (14d)$$

$$\underline{\theta}_w \leq \theta_w \leq \frac{\pi}{2}, \quad (14e)$$

where (14d) and (14e) jointly determine the constraints on the surveillance quality and the UAV operation scenario. Specifically, $d_w \leq \bar{d}_w$ guarantees that the UAV cannot be too far from Willie and $\underline{d}_w \leq \theta_w$ ensures that the UAV has an acceptable angle to Willie, which jointly guarantee a good surveillance quality. The constraint $\underline{d}_w \leq d_w$ is to avoid the UAV being visually observed by Willie. The constraint $\theta_w \leq \frac{\pi}{2}$ is due to the fact that the UAV will stay on the left side (where Bob locates) of Willie as shown in Fig. 1, rather than staying on the other side of Willie.

A. Optimal Location without Constraints

In order to solve the optimization problem (14), we first tackle the optimal d_w that maximizes $\gamma_b(P, d_w, \theta_w)$ for a given θ_w and the optimal θ_w that maximizes $\gamma_b(P, d_w, \theta_w)$ for a given d_w . We note that, if d_w and θ_w are jointly optimized, the UAV's optimal location that maximizes $\gamma_b(P, d_w, \theta_w)$ would be at Bob's location. In this subsection, we identify some properties on the optimal d_w for a given θ_w and the optimal θ_w for a given d_w , which will be used to facilitate solving the original optimization problem (14).

We first focus on the optimal d_w that maximizes $\gamma_b(P, d_w, \theta_w)$ for a given θ_w without any constraint. We recall that we have $\gamma_b(P, d_w, \theta_w) = Pf(d_w, \theta_w)/\sigma_b^2$, and thus maximizing $\gamma_b(P, d_w, \theta_w)$ is equivalent to maximizing

$f(d_w, \theta_w)$. As such, the corresponding optimization problem is given by

$$\operatorname{argmax}_{d_w} f(d_w, \theta_w), \quad (15)$$

where θ_w is fixed within $[0, \frac{\pi}{2}]$. We have the following lemma detailing the solution to the optimization problem (15).

Lemma 1: The solution to the optimization problem (15), i.e., the optimal value of d_w (denoted as $d_w^{\circ}(\theta_w)$) that maximizes $f(d_w, \theta_w)$ for a given θ_w , is unique and is given by the unique solution in d_w to the equation (16)

$$\xi_L [d_w - L \cos(\theta_w)] + \frac{180bL \sin(\theta_w)}{\pi} [1 - p_b(d_w, \theta_w)] = 0, \quad (16)$$

where $d_w^{\circ}(\theta_w)$ lies in the closed interval $[L \cos(\theta_w), L/\cos(\theta_w)]$, $\partial f(d_w, \theta_w)/\partial d_w > 0$ for $d_w \leq L \cos(\theta_w)$, and $\partial f(d_w, \theta_w)/\partial d_w < 0$ for $L/\cos(\theta_w) \leq d_w$.

Proof: The detailed proof is presented in Appendix A. ■

Intuitively, the results in Lemma 1 are due to the fact that, for a fixed $\theta_w < 90^\circ$, as the UAV moves away from Willie, the distance from the UAV to Bob, d_b , first decreases and then increases. Following Lemma 1, we note that the size of closed interval for the unique optimal d_w increases with θ_w , i.e., $d_w = L$ for $\theta_w = 0$ and $d_w \in [0, \infty]$ for $\theta_w = \pi/2$. We also note that the values of $L \cos(\theta_w)$ and $L/\cos(\theta_w)$ are critical, which divide the range of d_w into three subintervals. Explicitly, $f(d_w, \theta_w)$ monotonically increases with d_w for $\theta_w \in [0, L \cos(\theta_w)]$, and monotonically decreases with d_w for $\theta_w \in [L/\cos(\theta_w), \infty]$. The optimal d_w that maximizes $f(d_w, \theta_w)$ is therefore within $[L \cos(\theta_w), L/\cos(\theta_w)]$. In addition, following the uniqueness of the optimal d_w , we can conclude that $f(d_w, \theta_w)$ monotonically increases with d_w when $d_w \leq d_w^{\circ}(\theta_w)$ and $f(d_w, \theta_w)$ monotonically decreases with d_w when $d_w^{\circ}(\theta_w) \leq d_w$.

We now tackle the optimal θ_w that maximizes $\gamma_b(P, d_w, \theta_w)$ for a given d_w without any constraint. Noting $\gamma_b(P, d_w, \theta_w) = Pf(d_w, \theta_w)/\sigma_b^2$ again, the corresponding optimization problem is given by

$$\operatorname{argmax}_{\theta_w} f(d_w, \theta_w). \quad (17)$$

We have the following lemma detailing some properties of the solution to the optimization problem (17).

Lemma 2: When $d_w \leq L$ holds, the solution to the optimization problem (17), i.e., the optimal value of θ_w (denoted as $\theta_w^{\circ}(d_w)$) that maximizes $f(d_w, \theta_w)$ for a given d_w , is unique and is the unique solution in θ_w to the equation (18)

$$\xi_L L \sin(\theta_w) + \frac{180b}{\pi} \frac{\mathcal{G}(\theta_w)}{|L - d_w \cos(\theta_w)|} [1 - p_b(d_w, \theta_w)] = 0, \quad (18)$$

where $\mathcal{G}(\theta_w)$ given by

$$\mathcal{G}(\theta_w) = (L^2 + d_w^2) \cos(\theta_w) - d_w L [1 + \cos^2(\theta_w)]. \quad (19)$$

The optimal value, $\theta_w^{\circ}(d_w)$, lies in the closed interval $[0, \arccos(d_w/L)]$, and $\partial f(d_w, \theta_w)/\partial \theta_w < 0$ for $\arccos(d_w/L) \leq \theta_w$.

Proof: The detailed proof is presented in Appendix B. ■

Intuitively, the results in Lemma 2 are due to the fact that, for a fixed d_w with $d_w \leq L$, as the angle θ_w increases (i.e., the UAV flies higher while keeping the same distance to Willie), the distance from the UAV to Bob, d_b , monotonically increases, while the angle from the UAV to Bob, θ_b , first increases and then decreases with $\theta_w = \arccos(d_w/L)$ as the turning value. This is also the reason why the objective function monotonically decreases with θ_w for $\arccos(d_w/L) < \theta_w$. We note that the value of $\arccos(d_w/L)$ decreases with d_w , which means that the region where the UAV's optimal location belongs shrinks towards to Bob as d_w increases. We can conclude that the optimal location of the UAV is at Bob's location for $d_w = L$.

Lemma 3: When $d_w > L$ holds, the solution to the optimization problem (17), i.e., the optimal value of θ_w (denoted as $\theta_w^\circ(d_w)$) that maximizes $f(d_w, \theta_w)$ for a given d_w , is unique and is the unique solution in θ_w to the equation (20)

$$\xi_L L \sin(\theta_w) + \frac{180b}{\pi} \frac{\mathcal{G}(\theta_w)}{|L - d_w \cos(\theta_w)|} [1 - p_b(d_w, \theta_w)] = 0. \quad (20)$$

where $\mathcal{G}(\theta_w)$ is given by (19), $\theta_w^\circ(d_w)$ lies in the closed interval $[0, \arccos(L/d_w)]$, and the result $\partial f(d_w, \theta_w)/\partial \theta_w < 0$ holds for $\arccos(L/d_w) \leq \theta_w$.

Proof: The detailed proof is similar to that of Lemma 2, except that the angle $\arccos(L/d_w)$ is determined by solving $\mathcal{G}(\theta_w) = 0$ as per (19) within the value range of $\cos(\theta_w)$. ■

We note that the location $(d_w, \arccos(L/d_w))$ (in polar coordinates) is directly above Bob when $L < d_w$. Therefore, as per Lemma 3 we know that the UAV's optimal location is on the left side of Bob (while Willie is on the right side of Bob) as shown in Fig. 1. We next solve the original optimization problem (14) based on the results presented in Lemma 1, Lemma 2, and Lemma 3. We present the solution in six different scenarios with different relationships among \bar{d}_w , \underline{d}_w , $\underline{\theta}_w$, and L . Specifically, we gradually reduce the value of L (i.e., the distance between Bob and Willie) as we go from Scenario 1 to Scenario 6.

B. Scenario 1 with $\underline{d}_w < \bar{d}_w \leq L \cos(\underline{\theta}_w) < L/\cos(\underline{\theta}_w)$

This Scenario is depicted in Fig. 2(A) in which the distance between Bob and Willie, L , is much larger than \bar{d}_w . This is the most common scenario in practice, where Bob is a long way from the surveillance area.

As shown in Fig. 2(A), the light green region is the feasible set for the UAV's location, which is determined by the constraints $\underline{d}_w \leq d_w \leq \bar{d}_w$ and $\underline{\theta}_w \leq \theta_w \leq \frac{\pi}{2}$. The semi-circle with L as its diameter is determined by the locations of Bob and Willie. The points M, N and Q all lie on this semi-circle and are with different distances from Willie, which are $L \cos(\underline{\theta}_w)$, \bar{d}_w , and \underline{d}_w , respectively. Further, the angles $\angle BMW = \angle BNW = \angle BQW = 90^\circ$, $\angle BWN = \arccos(\bar{d}_w/L)$ and $\angle BWQ = \arccos(\underline{d}_w/L)$.

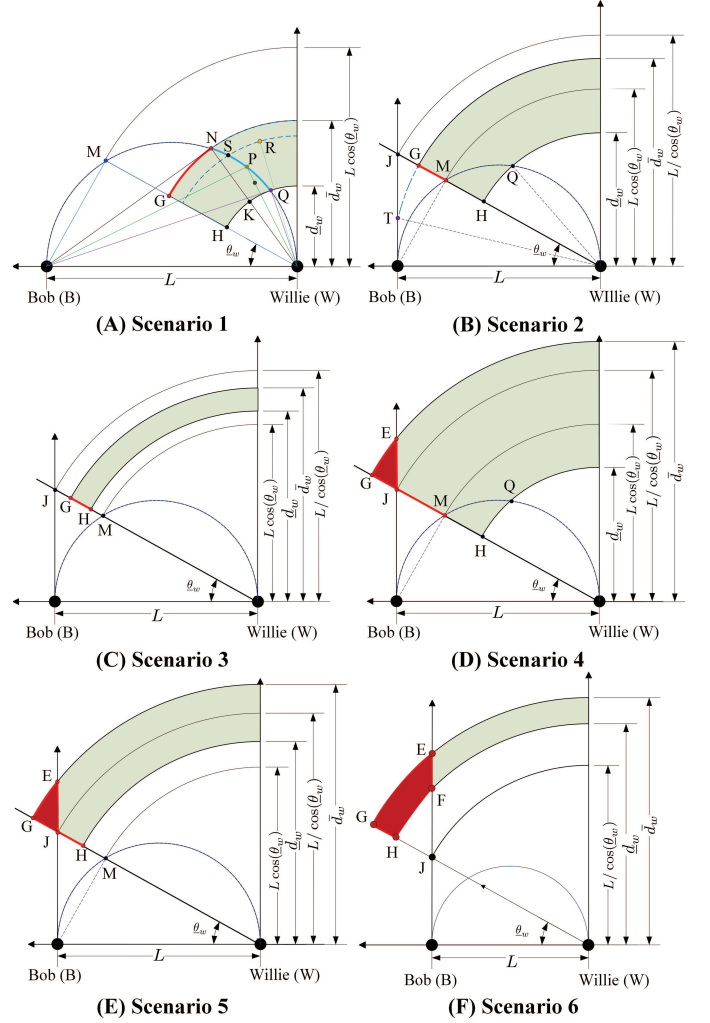


Fig. 2. The optimal location of the UAV is on the red line segment or within the region closed by the red line segments in six different scenarios.

Following (14), the optimization problem in the specific scenario as shown in Fig. 2(A) is

$$\operatorname{argmax}_{P, d_w, \theta_w} \gamma_b(P, d_w, \theta_w), \quad (21a)$$

$$\text{s.t. } \mathcal{D}_{01} \leq 2\epsilon^2, \quad (21b)$$

$$P \leq P_m, \quad (21c)$$

$$\underline{d}_w \leq d_w \leq \bar{d}_w, \quad (21d)$$

$$\underline{\theta}_w \leq \theta_w \leq \frac{\pi}{2}. \quad (21e)$$

In order to solve the above optimization problem, we first determine a feasible set of a significantly reduced size for the UAV's optimal location in the following theorem.

Theorem 1: The UAV's optimal location (d_w^*, θ_w^*) is on the arc GN shown in Fig. 2(A), i.e., $d_w^* = \bar{d}_w$ and θ_w^* satisfies $\underline{\theta}_w \leq \theta_w^* \leq \arccos(\bar{d}_w/L)$, regardless of the maximum transmit power constraint $P \leq P_m$.

Proof: We prove this theorem by first restricting the

feasible set of (d_w, θ_w) to the subset \mathcal{F} defined by

$$\mathcal{F} = \{(d_w, \theta_w) : \underline{d}_w \leq d_w \leq \bar{d}_w, \underline{\theta}_w \leq \theta_w < \arccos(\frac{\bar{d}_w}{L})\},$$

which is the green region to the left side of the straight line segment NK in Fig. 2(A). Over this subregion, we show that the optimal point must lie on the red arc GN. We then show that the optimal solution cannot lie outside of \mathcal{F} , i.e., it cannot lie in the green region on the right side of the line segment NK shown in Fig. 2(A).

For $(d_w, \theta_w) \in \mathcal{F}$, we have $L \cos(\theta_w) > d_w$, due to the following inequalities holding:

$$d_w \leq \bar{d}_w < L \cos(\underline{\theta}_w) < L \cos(\theta_w).$$

The second inequality holds because we are in Scenario 1. Lemma 1 shows that the objective function $\gamma_b(P, d_w, \theta_w)$ monotonically increases with d_w , for fixed θ_w , when $L \cos(\theta_w) > d_w$. We note that \mathcal{D}_{01} in the constraint (14b) is a monotonically decreasing function of d_w , since the received power $\bar{P} = P d_w^{\xi_L} p_w + P d_w^{\xi_N}$ (which appears in \mathcal{D}_{01}) decreases with d_w since $\xi_L < 0$ and $\xi_N < 0$. Considering the constraint $\underline{d}_w \leq d_w \leq \bar{d}_w$, we can conclude that \bar{d}_w is the optimal d_w for any given θ_w in this region, regardless of the maximum transmit power constraint, which means that the optimal solution within \mathcal{F} lies on the red arc GN.

We now show that the optimal solution cannot lie outside the subset \mathcal{F} . Note that if (d_w, θ_w) lies in the feasible region, but outside the set \mathcal{F} , then $\theta_w > \arccos(\bar{d}_w/L)$.

First, suppose that (d_w, θ_w) lies above the line segment NK but below the blue arc NQ. The point $(L \cos(\theta_w), \theta_w)$ has the same angle θ , but a greater distance from Willie, such that it lies on the blue arc (illustrated by point P in the Figure). By Lemma 1, the objective function is higher at P than at the considered point (d_w, θ_w) . Since \mathcal{D}_{01} in the constraint (14b) is a monotonically decreasing function of d_w , it follows that (d_w, θ_w) cannot be the optimal solution.

Next, consider a point (d_w, θ_w) that lies above the blue arc NQ, as illustrated by point R in Fig. 2(A). The point S has the same distance, d_w , from Willie as R, but a smaller angle, $\arccos(d_w/L)$, which means it lies on the blue arc NQ. Lemma 2 shows that $f(d_w, \theta_w)$ monotonically decreases with θ_w for a fixed d_w when $\theta_w > \arccos(d_w/L)$. Since \mathcal{D}_{01} monotonically increases with θ_w , we can conclude that the objective function value at the point S is higher than at point R, and the value of \mathcal{D}_{01} is smaller. It follows that the optimal solution cannot lie strictly above the blue arc NQ.

Finally, consider any point (d_w, θ_w) that lies on the blue arc NQ but strictly to the right of point N, i.e. with $d_w < \bar{d}_w$. Lemma 1 shows that such a point cannot be optimal, since the objective function increases with d_w for fixed angle θ_w , and \mathcal{D}_{01} decreases.

We conclude that the optimal solution must lie on the red arc GN. ■

Following Theorem 1, the solution to the optimization problem (21) is presented in the following proposition.

Proposition 1: The UAV's optimal location and transmit power that jointly maximize $\gamma_b(P, d_w, \theta_w)$ subject to the constraints (14b), (14c), (14d), and (14e), are given in Table I,

where we recall that $\theta_w^\circ(\bar{d}_w)$ is the optimal θ_w that maximizes $\gamma_b(P, \bar{d}_w, \theta_w)$ (obtained in Lemma 2), $\mathcal{D}_{01}(P, d_w, \theta_w)$ is the KL divergence \mathcal{D}_{01} , between \mathbb{P}_0 and \mathbb{P}_1 , as an explicit function of P , d_w , and θ_w , and P^ϵ is the unique value of P that ensures $\mathcal{D}_{01}(P, \bar{d}_w, \underline{\theta}_w) = 2\epsilon^2$. The values P^j and θ_w^j are the unique maximizers of the following optimization problem

$$\operatorname{argmax}_{P, \theta_w} \gamma_b(P, \bar{d}_w, \theta_w), \quad (22a)$$

$$\text{s.t. } \mathcal{D}_{01}(P, \bar{d}_w, \theta_w) = 2\epsilon^2, \quad (22b)$$

$$P \leq P_m, \quad (22c)$$

$$\max\{\underline{\theta}_w, \theta_w^\epsilon\} \leq \theta_w \leq \theta_w^\circ(\bar{d}_w), \quad (22d)$$

where θ_w^ϵ is the unique solution in θ_w to the equation $\mathcal{D}_{01}(P_m, \bar{d}_w, \theta_w) = 2\epsilon^2$.

TABLE I
SOLUTIONS TO THE OPTIMIZATION PROBLEM (21).

Solutions (d_w^*, θ_w^*, P^*)	Conditions
Case A: $(\bar{d}_w, \underline{\theta}_w, P_m)$	$\theta_w^\circ(\bar{d}_w) < \underline{\theta}_w$ $\mathcal{D}_{01}(P_m, \bar{d}_w, \underline{\theta}_w) \leq 2\epsilon^2$
Case B: $(\bar{d}_w, \underline{\theta}_w, P^\epsilon)$	$\theta_w^\circ(\bar{d}_w) < \underline{\theta}_w$ $\mathcal{D}_{01}(P_m, \bar{d}_w, \underline{\theta}_w) > 2\epsilon^2$
Case C: $(\bar{d}_w, \theta_w^\circ(\bar{d}_w), P_m)$	$\underline{\theta}_w \leq \theta_w^\circ(\bar{d}_w) \leq \arccos(\frac{\bar{d}_w}{L})$ $\mathcal{D}_{01}(P_m, \bar{d}_w, \theta_w^\circ(\bar{d}_w)) \leq 2\epsilon^2$
Case D: $(\bar{d}_w, \theta_w^j, P^j)$	$\underline{\theta}_w \leq \theta_w^\circ(\bar{d}_w) \leq \arccos(\frac{\bar{d}_w}{L})$ $\mathcal{D}_{01}(P_m, \bar{d}_w, \theta_w^\circ(\bar{d}_w)) > 2\epsilon^2$

Proof: When $\theta_w^\circ(\bar{d}_w) < \underline{\theta}_w$, we have $\theta_w^* = \underline{\theta}_w$, where we recall that $\theta_w^\circ(\bar{d}_w)$ is the optimal θ_w for $d_w = \bar{d}_w$ without any constraint. This is due to the fact that, with $\theta_w^\circ(\bar{d}_w) < \underline{\theta}_w$, both the objective function $\gamma_b(P, \bar{d}_w, \theta_w)$ and the KL divergence $\mathcal{D}_{01}(P, \bar{d}_w, \theta_w)$ monotonically decrease with θ_w for $\underline{\theta}_w \leq \theta_w \leq \arccos(\frac{\bar{d}_w}{L})$. In this case, if $\mathcal{D}_{01}(P_m, \bar{d}_w, \underline{\theta}_w) \leq 2\epsilon^2$, we have $P^* = P_m$. Otherwise, the optimal value of P is P^ϵ , which satisfies $\mathcal{D}_{01}(P, \bar{d}_w, \underline{\theta}_w) = 2\epsilon^2$.

We now focus on the case with $\underline{\theta}_w \leq \theta_w^\circ(\bar{d}_w) \leq \arccos(\frac{\bar{d}_w}{L})$. In this case, we have $\theta_w^* = \theta_w^\circ(\bar{d}_w)$ and $P^* = P_m$, if $\mathcal{D}_{01}(P_m, \bar{d}_w, \theta_w^\circ(\bar{d}_w)) \leq 2\epsilon^2$, which is due to the fact that the covertness constraint is not active at this point. In this case, if $\mathcal{D}_{01}(P_m, \bar{d}_w, \theta_w^\circ(\bar{d}_w)) > 2\epsilon^2$, the optimal values of θ_w and P are the ones that jointly maximize the objective function $\gamma_b(P, \bar{d}_w, \theta_w)$ subject to $\mathcal{D}_{01}(P, \bar{d}_w, \theta_w) \leq 2\epsilon^2$, $\max\{\underline{\theta}_w, \theta_w^\epsilon\} \leq \theta_w \leq \theta_w^\circ(\bar{d}_w)$, and $0 < P \leq P_m$. We note that the equality in $\mathcal{D}_{01}(P, \bar{d}_w, \theta_w) \leq 2\epsilon^2$ can always be satisfied, since the objective function $\gamma_b(P, \bar{d}_w, \theta_w)$ and the KL divergence $\mathcal{D}_{01}(P, \bar{d}_w, \theta_w)$ are both monotonically decreasing functions of θ_w , while they are monotonically increasing functions of the transmit power P . Specifically, the optimization problem is given in (22), which can be efficiently solved by a 1-dimensional search for θ_w over the interval $\underline{\theta}_w \leq \theta_w \leq \theta_w^\circ(\bar{d}_w)$ since P is uniquely determined by (22b). ■

In the following subsections we present the feasible regions of significantly reduced size for the UAV's optimal location for the remaining five scenarios. The proofs follow along similar lines to the proof of Theorem 1 but are omitted due to space considerations.

C. *Scenario 2 with $\underline{d}_w \leq L \cos(\underline{\theta}_w) \leq \bar{d}_w \leq L / \cos(\underline{\theta}_w)$*

As shown in Fig. 2(B), Scenario 2 with $\underline{d}_w \leq L \cos(\underline{\theta}_w) \leq \bar{d}_w \leq L / \cos(\underline{\theta}_w)$ is obtained by decreasing the distance, L , between Bob and Willie from that considered in Scenario 1. In Scenario 2, we can conclude that the optimal location of the UAV is on the line segment GM (shown in red) in Fig. 2(B), due to the following reasons.

- In the green shaded region with $\underline{d}_w \leq d_w \leq L \cos(\underline{\theta}_w)$ and $\underline{\theta}_w \leq \theta_w \leq \pi/2$, the best location of the UAV is on the point M, which follows from facts detailed in the proof of Theorem 1.
- In the region with $L \cos(\underline{\theta}_w) \leq d_w \leq \bar{d}_w$, the best location the UAV is on the line segment GM, which follows from results presented in Lemma 2 and Lemma 3.

D. *Scenario 3 with $L \cos(\underline{\theta}_w) \leq \underline{d}_w \leq \bar{d}_w \leq L / \cos(\underline{\theta}_w)$*

Following Scenario 2, if we further decrease the distance, L , between Bob and Willie, we may have $L \cos(\underline{\theta}_w) \leq \underline{d}_w \leq \bar{d}_w \leq L / \cos(\underline{\theta}_w)$ which is Scenario 3 as shown in Fig. 2(C). Alternatively, we may have $\underline{d}_w \leq L \cos(\underline{\theta}_w) < L / \cos(\underline{\theta}_w) \leq \bar{d}_w$ which is Scenario 4 in Fig. 2(D).

In Scenario 3, for any possible location within the green region on the right side of the line segment GH, we can find one location on the line segment GH that achieves a higher objective function $\gamma_b(P, d_w, \theta_w)$. This is due to the following two facts.

- For any given fixed d_w within this area (i.e., the green region in Fig. 2(C)), the distance to Bob, d_b , increases with θ_w , while the angle to Bob, θ_b , monotonically decreases with θ_w (due to that there is no intersection between the green region and the semi-circle), which leads to that the objective function $\gamma_b(P, d_w, \theta_w)$ monotonically decreases with θ_w for any fixed d_w in the green region.
- The KL divergence \mathcal{D}_{01} is a monotonically increasing function of θ_w for any fixed d_w in the green region, since the probability p_w to have the LoS component in the channel from the UAV to Willie monotonically increases with θ_w .

Therefore, we can conclude that the optimal location of the UAV is on the line segment GH in this scenario. We also note that, if the covertness constraint can be satisfied with $P = P_m$ at the point H, we can conclude that the optimal location is on the point H. This is due to the fact that, for a fixed transmit power, both the objective function $\gamma_b(P, d_w, \theta_w)$ and the KL divergence \mathcal{D}_{01} in the covertness constraint $\mathcal{D}_{01} \leq 2\epsilon^2$ monotonically decrease with d_w on the line segment GH, as shown in Lemma 1.

E. *Scenario 4 with $\underline{d}_w \leq L \cos(\underline{\theta}_w) < L / \cos(\underline{\theta}_w) \leq \bar{d}_w$*

Scenario 4 can arise instead of Scenario 3, from decreasing L from Scenario 2. Scenario 4 occurs if $\underline{d}_w \leq L \cos(\underline{\theta}_w) < L / \cos(\underline{\theta}_w) \leq \bar{d}_w$ when decreasing L from Scenario 2. Scenario 4 is illustrated in Fig. 2(D). In this scenario, we can conclude that the optimal location of the UAV is within the region EGJ or on the line segment JM (shown in red), due to Lemma 3 and Theorem 1.

F. *Scenario 5 with $L \cos(\underline{\theta}_w) \leq \underline{d}_w \leq L / \cos(\underline{\theta}_w) \leq \bar{d}_w$*

If we further decrease the distance, L , between Bob and Willie, beyond Scenario 3 or 4, we will have $L \cos(\underline{\theta}_w) \leq \underline{d}_w \leq L / \cos(\underline{\theta}_w) \leq \bar{d}_w$, which is Scenario 5 as shown in Fig. 2(E). In this scenario, we can conclude that the optimal location of the UAV is within the region EGJ or on the line segment JH (shown in red), due to similar reasons for achieving the results in Scenario 4.

G. *Scenario 6 with $L \cos(\underline{\theta}_w) < L / \cos(\underline{\theta}_w) \leq \underline{d}_w < \bar{d}_w$*

Following Scenario 5, if we continue to reduce L , we will obtain Scenario 6 with $L \cos(\underline{\theta}_w) < L / \cos(\underline{\theta}_w) \leq \underline{d}_w < \bar{d}_w$ as shown in Fig. 2(F). In this scenario, following Lemma 3 and the discussions on Scenario 5, we can conclude that the UAV's optimal location is on the left side of Bob, i.e., within the closed region GEFH.

H. Heuristic Approaches

From a practical point of view, two simple alternatives to solving (14) present themselves. The first is to simply fly the UAV at the closest point to Bob within the feasible region, regardless of the scenario. The second is to choose the point in the feasible region with the largest angle to Bob, since this maximizes the probability of a LoS to Bob. In Section V, we compare these heuristic suboptimal approaches with our approach, and show that in some cases they are able to achieve close to optimal, but that in other cases significant gains can be achieved by employing our optimal approaches.

I. Summary of Results

The following general conclusions provide a summary of the results from the six scenarios.

- As long as the whole feasible region of the optimal location is on the upper right side of Bob, the 2-dimensional location optimization problem reduces to a 1-dimensional optimization problem, which can be seen from Scenarios 1, 2, and 3 as shown in Fig. 2.
- We note that Scenario 1 is the most common scenario, where Bob is far from Willie and thus the wireless communication from the UAV to Bob is desirable for conveying urgent information about the surveillance outcomes. However, in this work we consider all the scenarios to present a whole picture about the UAV's location optimization for covert wireless communications.

IV. OPTIMAL HEIGHT AND TRANSMIT POWER FOR A VERTICAL UAV

In this section, we focus on a special scenario with a vertical UAV, i.e., the UAV can only adjust its flying height. This scenario arises if the surveillance equipment (e.g., a camera) can only undertake its surveillance tasks when the UAV is directly above the target. We note that this is a special case of Scenario 3 discussed in the previous section by setting $\underline{\theta}_w = 90^\circ$. Considering this vertical UAV, in this section we determine the optimal height, h , and transmit power, P .

We denote the lower and upper bounds on the height by \underline{h} , and \bar{h} , respectively. To simplify the presentation, we denote the effective SNR (denoted as $\gamma_b(P, d_w, \theta_w)$ in the previous section) as $\gamma_b(P, h)$ in this section.

A. Optimal Height without Any Constraint

In order to determine the optimal height and transmit power of the UAV to conduct covert transmission, similar to Section II-A, in this subsection we derive the optimal height of the UAV for transmitting to Bob without any constraint. We note that there is an optimal height for the UAV Alice, which maximizes the effective SNR $\gamma_b(P, h)$ at Bob, since both d_b and p_b monotonically increase with h . To facilitate determining the optimal height of the UAV with a covertness constraint, we first identify the optimal height h that maximizes $\gamma_b(P, h)$ for a given transmit power P . The corresponding optimization problem is given by

$$\operatorname{argmax}_h \gamma_b(P, h), \quad (23)$$

where we recall that $\gamma_b(P, h) = Pd_b^{\xi_L} p_b / \sigma_b^2$ and p_b is given in (2). Following Lemma 1, the solution to the optimization problem (23) is given in the following lemma.

Lemma 4: The optimal h , which we denote by h^\dagger , that maximizes $\gamma_b(P, h)$ is the unique solution to the following fixed-point equation:

$$h = -\frac{180bL}{\pi\xi_L} \left[1 - \frac{1}{1 + a \exp(-b[\frac{180}{\pi} \tan^{-1}(\frac{h}{L}) - a])} \right]. \quad (24)$$

Proof: Obtained from Lemma 1 by setting $\theta_w = 90^\circ$. ■

From Lemma 4, we note that the optimal height h^\dagger of the UAV without any constraint is independent of the UAV's transmit power P and the AWGN variance at Bob (i.e., σ_b^2), and is solely determined by the environment parameters (e.g., ξ_L , a , b , and L).

B. Optimal Height with Covertness, Transmit Power, and Surveillance Constraints

The optimization problem at the UAV is given by

$$\operatorname{argmax}_{P, h} \gamma_b(P, h), \quad (25a)$$

$$\text{s.t. } \mathcal{D}_{01} \leq 2\epsilon^2, \quad (25b)$$

$$P \leq P_m, \quad (25c)$$

$$h \leq \bar{h}, \quad (25d)$$

$$h \geq \underline{h}, \quad (25e)$$

where we recall that \bar{h} is the maximum value of the UAV's height, and \underline{h} is the minimum value.

In order to facilitate presenting the solution to the optimization problem (25), we first write \mathcal{D}_{01} as an explicit function of h and P , which is $\mathcal{D}_{01}(P, h)$. Following (9), we note that, for a fixed P and $p_w = 1$ due to $\theta_w = 90^\circ$, $\mathcal{D}_{01}(P, h)$ is a monotonically decreasing function of h , since, for a fixed transmit power P , the received power $\bar{P} = Pd_w^{\xi_L} p_w + Pd_w^{\xi_N}$ in (9) monotonically decreases with h . We denote the unique solution of h to $\mathcal{D}_{01}(P_m, h) = 2\epsilon^2$ as h^\ddagger , where we recall that

P_m is the maximum transmit power of the UAV. Likewise, $\mathcal{D}_{01}(P, h)$ is a monotonically increasing function of P for a fixed h . As such, we denote the unique solution of P to $\mathcal{D}_{01}(P, \bar{h}) = 2\epsilon^2$ as P^\dagger , where we recall that \bar{h} is the upper bound on h (i.e., $h \leq \bar{h}$). We note that h^\ddagger and P^\dagger can be approximately achieved in closed-form expressions by using a similar approach presented in [25]. We next present the solution to the optimization problem (25) in the following theorem.

Theorem 2: The optimal height h^* and the optimal transmit power P^* that jointly maximize $\gamma_b(P, h)$ subject to the constraints (14b), (14c), (25d), and (25e) are given in Table II as below.

TABLE II
SOLUTIONS TO THE OPTIMIZATION PROBLEM (25).

Solutions (h^*, P^*)	Conditions
Case 1: (\underline{h}, P_m)	$h^\dagger \leq \underline{h}$ and $h^\ddagger \leq \underline{h}$
Case 2: (h^\ddagger, P_m)	$\underline{h} < h^\ddagger < \bar{h}$ and $h^\dagger < h^\ddagger$
Case 3: (h, P^\dagger)	$h^\ddagger \geq \bar{h}$
Case 4: (h^\dagger, P_m)	$\underline{h} < h^\dagger < \bar{h}$ and $h^\ddagger < h^\dagger$
Case 5: (h, P_m)	$h^\dagger \geq \bar{h}$ and $h^\ddagger \leq \bar{h}$

Proof: The detailed proof can be found in our conference version of this work [1]. ■

Following Theorem 2, we note that the UAV's optimal height with covertness constraint h^* is indeed a function of its transmit power, although its optimal height without any constraint is independent of its transmit power as shown in Lemma 4. We also note that, when the maximum transmit power of the UAV is sufficiently large, we should have the solution in Case 3, since h^\ddagger is the solution to $\mathcal{D}_{01}(P_m, h) = 2\epsilon^2$ and it monotonically increases with P_m as per (9). As expected, from Theorem 2 we can see that h^* is a function of h^\ddagger , which leads to the fact that h^* highly depends on the covertness constraint (i.e., the value of ϵ).

V. NUMERICAL RESULTS

In Fig. 3, we plot the UAV's optimal location for different values of L , the distance between Bob and Willie, where the region bounded by the solid green lines is the feasible region for the UAV's location. We use a dashed line to connect each of Bob's locations to the corresponding UAV's optimal location. If we consider the locations in sequence, as we decrease L from 10 km to 0.5 km, we observe that the optimal point moves from a location that is the maximum distance from Willie to the minimum distance. At the first two points (when $L = 10$ km, and $L = 9.5$ km, respectively) we are in Scenario 1, and the maximum distance constraint is tight as is always the case in Scenario 1. The lower bound on the angle is not tight in these two cases, due to the fact that the probability of a LoS component to Bob is higher as the UAV flies higher. At the next point (on the corner, which corresponds to Scenario 2 in this case) the lower bound on the angle becomes tight. It remains tight for all the remaining points shown (which correspond to Scenarios 4, 5, and 6). At the last point (when $L = 0.5$ km, which is in Scenario 6 in this case) the minimum

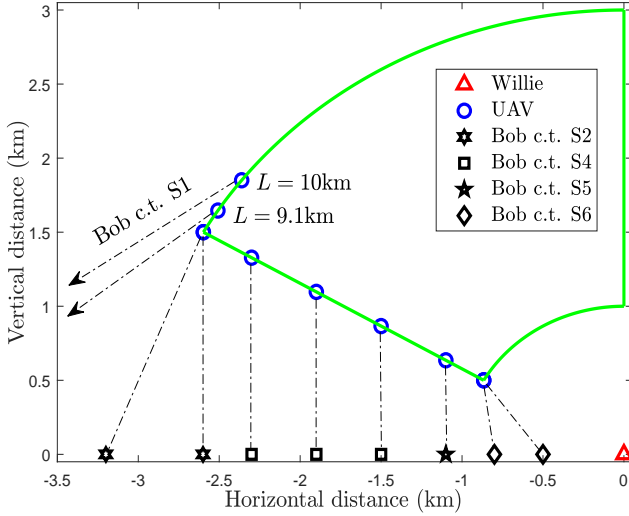


Fig. 3. The optimal location of the UAV for different values of the distance, L , between Bob and Willie, corresponding to (c.t.) different scenarios, where $a = 4.88$, $b = 0.429$, $\xi_L = -2$, $\xi_N = -3$, $P_m = 20\text{dB}$, $\epsilon = 0.01$, $\sigma_b^2 = -90\text{dB}$, $\sigma_w^2 = -60\text{dB}$, $n = 200$, $\underline{\theta}_w = \pi/6$, $\bar{d}_w = 3\text{km}$, and $\underline{d}_w = 1\text{km}$.

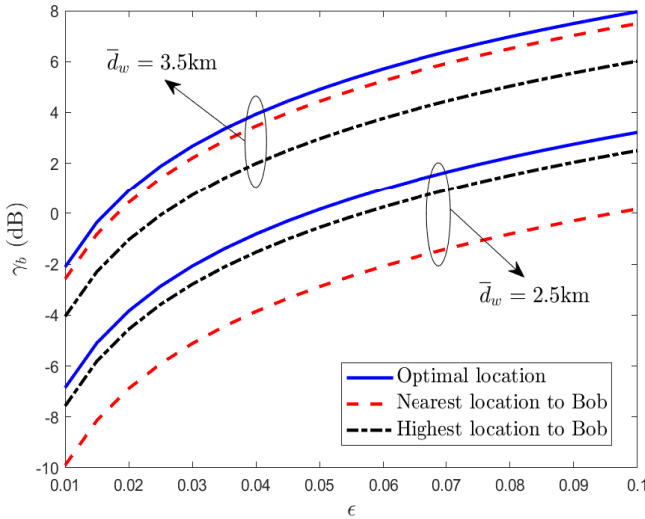


Fig. 4. SNR, γ_b , versus ϵ , for $L = 10\text{km}$, $P_m = 10\text{dBm}$, $\sigma_b^2 = -90\text{dBm}$, $\sigma_w^2 = -60\text{dBm}$, $n = 200$, $\underline{\theta}_w = \pi/8$, $\bar{d}_w = 3\text{km}$, and $\underline{d}_w = 1\text{km}$, and with channel parameters $a = 4.88$, $b = 0.429$, $\xi_L = -2$, $\xi_N = -3$.

distance constraint has become tight. We also observe that the UAV's optimal location is always on the border of the feasible region under the specific simulation settings of this figure. Note that in one case (in Scenario 6) the optimal solution is to fly the UAV at the nearest feasible location to Bob, and for others (Scenarios 4 and 5) the optimal location is almost directly above Bob (which is the closest point in the feasible region with the highest angle to Bob).

Fig. 4 considers Scenario 1, and shows the achieved optimal values of Bob's effective SNR γ_b when the UAV is in the optimal location. We observe that the optimal γ_b monotonically increases with ϵ . This is due to the fact that the maximum transmit power constraint is not active and the optimal transmit

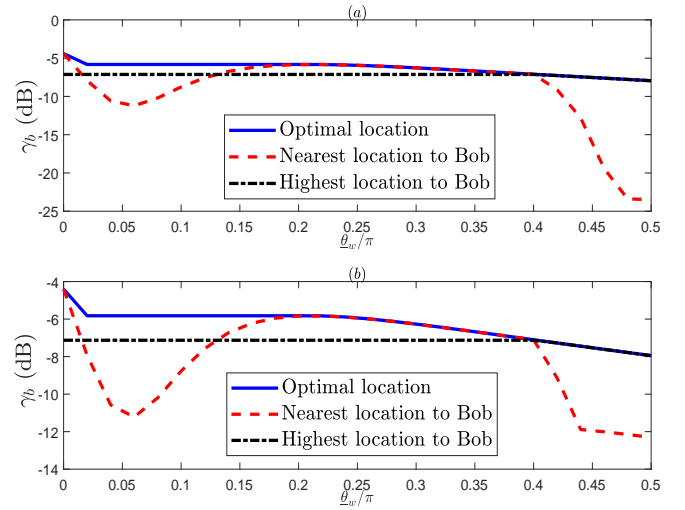


Fig. 5. SNR, γ_b , versus ϵ for (a) $L = 10\text{km}$ and (b) $L = 15\text{km}$. With $P_m = 10\text{dBm}$, $\epsilon = 0.1$, $\sigma_b^2 = -90\text{dBm}$, $\sigma_w^2 = -60\text{dBm}$, $n = 200$, $\underline{d}_w = 1\text{km}$, $\bar{d}_w = 3\text{km}$, and with channel parameters $a = 4.88$, $b = 0.429$, $\xi_L = -2$, $\xi_N = -3$.

power increases with ϵ (as the covertness constraint becomes less onerous). We also plot the values of Bob's effective SNR for the two heuristic approaches described in Section III-H. We observe that neither heuristic scheme is optimal in general. When the distance to Willie is upper bounded by 3.5 km, the nearest location to Bob is the better of the two. When the upper bound is 2.5 km, the location with the highest angle to Bob is the better one. Additional numerical results, not reported here, suggest a third heuristic approach would be to calculate both heuristic approaches and pick the best, although this is still not optimal.

Fig. 5 plots the optimal SNR as a function of the lower angle constraint $\underline{\theta}_w$, for two different values of L . Note that $\underline{\theta}_w/\pi = 0.5$ corresponds to the vertical UAV scenario where there is only one degree of freedom: the UAV's height. We observe that the optimal value of γ_b monotonically decreases with $\underline{\theta}_w$. The figure also shows results for the two heuristic schemes described in Section III-H. We observe that neither heuristic scheme is optimal across the whole range of $\underline{\theta}_w$.

In Fig. 6, we consider the vertical UAV scenario. Specifically, we plot possible values of the UAV's height h versus the covertness parameter ϵ , where we recall that a smaller ϵ represents a stricter covertness constraint. As expected, in this figure we first observe that neither h^\dagger nor \bar{h} is a function of ϵ , while h^\ddagger is indeed a function of ϵ . We also observe that h^\ddagger monotonically decreases with ϵ , which leads to the fact that the solutions to the optimal h and P move from Case 3 to Case 2 and then to Case 4 as ϵ increases. We note that in Case 3 and Case 4 we have $D_{01} < 2\epsilon^2$, while in Case 2 we have $D_{01} = 2\epsilon^2$. This is the reason why in Case 3 and Case 4 the optimal height h^* does not directly depend on ϵ , while in Case 2 we have that h^* monotonically decreases with ϵ . In general, this figure shows that the UAV's optimal height with covertness constraint decreases with ϵ .

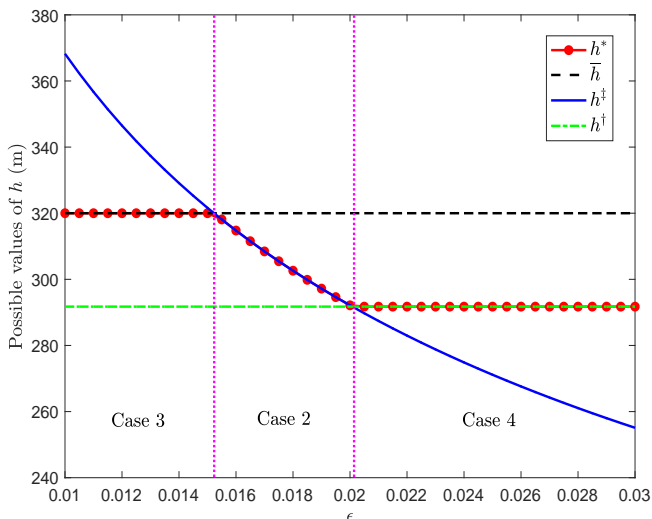


Fig. 6. Possible values of UAV's height versus the covertness parameter ϵ , where the S-curve parameters are $a = 4.88$ and $b = 0.429$, the path loss exponent is $\xi = -3$, the UAV's maximum transmit power is $P_m = 10\text{dBm}$, the AWGN power is $\sigma_w^2 = -40\text{dBm}$, the distance from Bob to Willie is $L = 100\text{m}$, the number of the channel uses is $n = 200$, and the lower bound on the UAV's height is $\underline{h} = 100\text{m}$.

VI. CONCLUSION

We have shown that covertness constraints on UAV communications in surveillance applications leads to six possible scenarios, with corresponding feasibility regions for the flying location of the UAV. We showed that these regions can be searched efficiently to find the optimal flying height and ground distance between the legitimate ground station and a potential eaves dropper. We discussed two heuristic approaches to UAV placement, and showed that in some cases they are able to achieve close to optimal, but that in other cases significant gains can be achieved by employing our new search techniques.

ACKNOWLEDGEMENT

We thank Prof. Dennis Goeckel for his contribution to the vertical UAV case in Section IV.

APPENDIX A: PROOF OF LEMMA 1

Proof: Following (13), the first derivative of $f(d_w, \theta_w)$ with respect to d_w is derived as

$$\begin{aligned} \frac{\partial f(d_w, \theta_w)}{\partial d_w} &= \frac{p_b(d_w, \theta_w) \xi_L [d_w - L \cos(\theta_w)]}{[L^2 + d_w^2 - 2d_w L \cos(\theta_w)]^{1 - \frac{\xi_L}{2}}} + p_b^2(d_w, \theta_w) \\ &\quad [L^2 + d_w^2 - 2d_w L \cos(\theta_w)]^{\frac{\xi_L}{2}} \frac{180}{\pi} ab \\ &\quad \times \exp \left\{ -b \left[\frac{180}{\pi} \sin^{-1} \left(\frac{d_w \sin(\theta_w)}{\sqrt{L^2 + d_w^2 - 2d_w L \cos(\theta_w)}} \right) \right] - a \right\} \\ &\quad \times \frac{\sin(\theta_w)}{|L - d_w \cos(\theta_w)|} \times \frac{L[L - d_w \cos(\theta_w)]}{L^2 + d_w^2 - 2d_w L \cos(\theta_w)}, \end{aligned} \quad (26)$$

$$= p_b(d_w, \theta_w) [L^2 + d_w^2 - 2d_w L \cos(\theta_w)]^{\frac{\xi_L}{2} - 1} \bar{f}(d_w), \quad (27)$$

where $p_b(d_w, \theta_w)$ is the probability to have the LoS component in the channel from the UAV to Bob, given by

$$p_b(d_w, \theta_w) = \frac{1}{1 + a \exp \left\{ -b \left[\frac{180}{\pi} \sin^{-1} \left(\frac{d_w \sin(\theta_w)}{\sqrt{L^2 + d_w^2 - 2d_w L \cos(\theta_w)}} \right) \right] - a \right\}}, \quad (28)$$

and

$$\begin{aligned} \bar{f}(d_w) &= \xi_L [d_w - L \cos(\theta_w)] + p_b(d_w, \theta_w) \sin(\theta_w) \\ &\quad \times \frac{180ab}{\pi} \frac{L[L - d_w \cos(\theta_w)]}{|L - d_w \cos(\theta_w)|} \\ &\quad \times \exp \left\{ -b \left[\frac{180}{\pi} \sin^{-1} \left(\frac{d_w \sin(\theta_w)}{\sqrt{L^2 + d_w^2 - 2d_w L \cos(\theta_w)}} \right) \right] - a \right\} \\ &= \xi_L [d_w - L \cos(\theta_w)] + \sin(\theta_w) \\ &\quad \times \frac{180b}{\pi} \frac{L[L - d_w \cos(\theta_w)]}{|L - d_w \cos(\theta_w)|} [1 - p_b(d_w, \theta_w)]. \end{aligned} \quad (29)$$

Considering $p_b(d_w, \theta_w) > 0$ and $L^2 + d_w^2 - 2d_w L \cos(\theta_w) = d_b^2 > 0$, following (27) we note that the solution of d_w to $\partial f(d_w, \theta_w) / \partial d_w = 0$ is the same as the solution to $\bar{f}(d_w) = 0$. We also note that we have $\xi_L < 0$, $\sin(\theta_w) > 0$ due to $0 \leq \theta_w \leq \frac{\pi}{2}$, and $p_b(d_w, \theta_w) < 1$ in (29). As such, as per (29) we have $\bar{f}(d_w) < 0$ when $d_w > L / \cos(\theta_w)$, which leads to the conclusion of having $\partial f(d_w, \theta_w) / \partial d_w < 0$ for $d_w > L / \cos(\theta_w)$ according to (27). Likewise, we have another conclusion of having $\partial f(d_w, \theta_w) / \partial d_w > 0$ for $d_w < L \cos(\theta_w)$. These two conclusions lead to that the solution to $\partial f(d_w, \theta_w) / \partial d_w = 0$ is in the closed interval $[L \cos(\theta_w), L / \cos(\theta_w)]$. In this closed interval, following (29) the function $\bar{f}(d_w)$ can be simplified as

$$\bar{f}(d_w) = \xi_L [d_w - L \cos(\theta_w)] + \frac{180bL \sin(\theta_w)}{\pi} [1 - p_b(d_w, \theta_w)]. \quad (30)$$

We next prove that this solution is unique. To this end, we first derive the first derivative of $p_b(d_w, \theta_w)$ with respect to d_w as

$$\begin{aligned} \frac{\partial p_b(d_w, \theta_w)}{\partial d_w} &= p_b^2(d_w, \theta_w) [L^2 + d_w^2 - 2d_w L \cos(\theta_w)]^{-1} \frac{180}{\pi} ab \\ &\quad \times \exp \left\{ -b \left[\frac{180}{\pi} \sin^{-1} \left(\frac{d_w \sin(\theta_w)}{\sqrt{L^2 + d_w^2 - 2d_w L \cos(\theta_w)}} \right) \right] - a \right\} \\ &\quad \times \frac{\sin(\theta_w) L [L - d_w \cos(\theta_w)]}{|L - d_w \cos(\theta_w)|}. \end{aligned} \quad (31)$$

Following (31), we note that $\partial p_b(d_w, \theta_w) / \partial d_w > 0$ in the closed interval $[L \cos(\theta_w), L / \cos(\theta_w)]$. Noting $\xi_L < 0$ and following (30), we can see that $\bar{f}(d_w)$ monotonically decreases with d_w in the interval $[L \cos(\theta_w), L / \cos(\theta_w)]$, which leads to the fact that the solution to $\bar{f}(d_w) = 0$ is unique and thus the solution to $\partial f(d_w, \theta_w) / \partial d_w = 0$ is also unique in the closed interval $[L \cos(\theta_w), L / \cos(\theta_w)]$. This completes the proof of this lemma. \blacksquare

APPENDIX B: PROOF OF LEMMA 2

The first derivative of $f(d_w, \theta_w)$ with respect to θ_w is derived as

$$\begin{aligned} \frac{\partial f(d_w, \theta_w)}{\partial \theta_w} &= \frac{p_b(d_w, \theta_w) \xi_L d_w L \sin(\theta_w)}{[L^2 + d_w^2 - 2d_w L \cos(\theta_w)]^{1 - \frac{\xi_L}{2}}} + p_b^2(d_w, \theta_w) \\ &\quad \times [L^2 + d_w^2 - 2d_w L \cos(\theta_w)]^{\frac{\xi_L}{2}} \frac{180}{\pi} ab \\ &\quad \times \exp \left\{ -b \left[\frac{180}{\pi} \sin^{-1} \left(\frac{d_w \sin(\theta_w)}{\sqrt{L^2 + d_w^2 - 2d_w L \cos(\theta_w)}} \right) \right] - a \right\} \\ &\quad \times \frac{d_w}{|L - d_w \cos(\theta_w)|} \frac{(L^2 + d_w^2) \cos(\theta_w) - d_w L [1 + \cos^2(\theta_w)]}{L^2 + d_w^2 - 2d_w L \cos(\theta_w)} \end{aligned} \quad (32)$$

$$= p_b(d_w, \theta_w) d_w [L^2 + d_w^2 - 2d_w L \cos(\theta_w)]^{\frac{\xi_L}{2} - 1} \times \bar{g}(\theta_w), \quad (33)$$

where

$$\begin{aligned} \bar{g}(\theta_w) &= \xi_L L \sin(\theta_w) + p_b(d_w, \theta_w) \frac{180ab}{\pi} \\ &\quad \times \frac{(L^2 + d_w^2) \cos(\theta_w) - d_w L [1 + \cos^2(\theta_w)]}{|L - d_w \cos(\theta_w)|} \\ &\quad \times \exp \left\{ -b \left[\frac{180}{\pi} \sin^{-1} \left(\frac{d_w \sin(\theta_w)}{\sqrt{L^2 + d_w^2 - 2d_w L \cos(\theta_w)}} \right) \right] - a \right\} \\ &= \xi_L L \sin(\theta_w) + \frac{180b}{\pi} \frac{\mathcal{G}(\theta_w)}{|L - d_w \cos(\theta_w)|} [1 - p_b(d_w, \theta_w)]. \end{aligned} \quad (34)$$

Considering $p_b(d_w, \theta_w) > 0$, $L^2 + d_w^2 - 2d_w L \cos(\theta_w) = d_b^2 > 0$, and $d_w > 0$, following (32) we note that the solution of θ_w to $\partial f(d_w, \theta_w)/\partial \theta_w = 0$ is the same as the solution of d_w to $\bar{g}(\theta_w) = 0$. We next determine the value range of the optimal θ_w . Following (19), the first derivative of $\mathcal{G}(\theta_w)$ with respect to θ_w is derived as

$$\begin{aligned} \frac{\partial \mathcal{G}(\theta_w)}{\partial \theta_w} &= -(L^2 + d_w^2) \sin(\theta_w) + 2d_w L \sin(\theta_w) \cos(\theta_w) \\ &= -\sin(\theta_w) d_b^2 < 0, \end{aligned} \quad (35)$$

which indicates that $\mathcal{G}(\theta_w)$ monotonically decreases with θ_w . We note that $\mathcal{G}(\arccos(d_w/L)) = 0$ when $d_w \leq L$ holds, and thus following (19) we have $\mathcal{G}(\theta_w) < 0$ for $\theta_w \geq \arccos(d_w/L)$ and $\mathcal{G}(\theta_w) > 0$ for $\theta_w < \arccos(d_w/L)$. Following (34) and noting $\xi_L < 0$, $\sin(\theta_w) > 0$, and $1 - p_b(d_w, \theta_w) > 0$, we know that $\bar{g}(\theta_w) = 0$ requires $\mathcal{G}(\theta_w) > 0$, which requires $\theta_w < \arccos(d_w/L)$. As such, we can conclude that the solution to $\bar{g}(\theta_w) = 0$ is within the closed interval $[0, \arccos(d_w/L)]$.

In the following, we prove that the solution is unique within the interval $[0, \arccos(d_w/L)]$. To this end, we derive the first derivative of $p_b(d_w, \theta_w)$ with respect to θ_w as

$$\begin{aligned} \frac{\partial p_b(d_w, \theta_w)}{\partial \theta_w} &= p_b^2(d_w, \theta_w) \frac{180}{\pi} ab \exp \left\{ -b \left[\frac{180}{\pi} \right. \right. \\ &\quad \times \sin^{-1} \left(\frac{d_w \sin(\theta_w)}{\sqrt{L^2 + d_w^2 - 2d_w L \cos(\theta_w)}} \right) \left. \left. \right] - a \right\} \\ &\quad \times \frac{d_w}{|L - d_w \cos(\theta_w)|} \frac{\mathcal{G}(\theta_w)}{L^2 + d_w^2 - 2d_w L \cos(\theta_w)}. \end{aligned} \quad (36)$$

Considering the values of $\mathcal{G}(\theta_w)$ discussed below (35), following (36) we have $\partial p_b(d_w, \theta_w)/\partial \theta_w > 0$ for $\theta_w \leq \arccos(d_w/L)$, which demonstrates that $p_b(d_w, \theta_w)$ monotonically increases with θ_w for $\theta_w \leq \arccos(d_w/L)$ and thus $1 - p_b(d_w, \theta_w) > 0$ monotonically decreases with θ_w for $\theta_w \leq \arccos(d_w/L)$. We note that $\xi_L \sin(\theta_w)$ monotonically decreases with θ_w due to $\xi_L < 0$. In addition, as per (35) and its following discussions, we know that $\mathcal{G}(\theta_w) > 0$ and $\mathcal{G}(\theta_w)$ monotonically decreases with θ_w for $\theta_w < \arccos(d_w/L)$. Furthermore, $1/|L - d_w \cos(\theta_w)|$ monotonically decreases with θ_w for $L - d_w \cos(\theta_w) > 0$. Therefore, following (34), we can conclude that $\bar{g}(\theta_w)$ monotonically decreases with θ_w within the closed interval $[0, \arccos(d_w/L)]$ when $L - d_w \cos(\theta_w) > 0$, which leads to that the solution to $\bar{g}(\theta_w) = 0$ is unique within the interval $[0, \arccos(d_w/L)]$ for $L - d_w \cos(\theta_w) > 0$.

We recall that we have $\mathcal{G}(\theta_w) < 0$ for $\theta_w \geq \arccos(d_w/L)$ according to (35) and its following discussions. Then, following (34), and noting $\xi_L < 0$ and $1 - p_b(d_w, \theta_w) > 0$, we have $\bar{g}(\theta_w) < 0$ and thus $\partial f(d_w, \theta_w)/\partial \theta_w < 0$ for $\theta_w \geq \arccos(d_w/L)$, which indicates that $f(d_w, \theta_w)$ monotonically decreases with θ_w for $\arccos(d_w/L) \leq \theta_w \leq \frac{\pi}{2}$ and thus completes the proof.

REFERENCES

- [1] S. Yan, S. V. Hanly, I. B. Collings, and D. L. Goeckel, "Hiding unmanned aerial vehicles for wireless transmissions by covert communications," in *Proc. IEEE International Conference on Communications (ICC)*, May 2019, pp. 1–6.
- [2] K. P. Valavanis and G. J. Vachtsevanos, *Handbook of Unmanned Aerial Vehicles*, 2015.
- [3] Y. Zeng, R. Zhang, and T. J. Lim, "Wireless communications with unmanned aerial vehicles: Opportunities and challenges," *IEEE Commun. Mag.*, vol. 54, no. 5, pp. 36–42, May 2016.
- [4] Q. Wu, Y. Zeng, and R. Zhang, "Joint trajectory and communication design for multi-UAV enabled wireless networks," *IEEE Trans. Wireless Commun.*, vol. 17, no. 3, pp. 2109–2121, Mar. 2018.
- [5] A. Al-Hourani, S. Kandeepan, and S. Lardner, "Optimal lap altitude for maximum coverage," *IEEE Wireless Commun. Lett.*, vol. 3, no. 6, pp. 569–572, Dec. 2014.
- [6] D. Xu, Y. Sun, D. W. K. Ng, and R. Schober, "Multiuser MISO UAV communications in uncertain environments with no-fly zones: Robust trajectory and resource allocation design," *IEEE Trans. Commun.*, vol. 68, no. 5, pp. 3153–3172, May 2020.
- [7] P. Li and J. Xu, "Fundamental rate limits of UAV-enabled multiple access channel with trajectory optimization," *IEEE Trans. Wireless Commun.*, vol. 19, no. 1, pp. 458–474, Jan. 2020.
- [8] Q. Wang, Z. Chen, W. Mei, and J. Fang, "Improving physical layer security using UAV-enabled mobile relaying," *IEEE Wireless Commun. Lett.*, vol. 6, no. 3, pp. 310–313, Jun. 2017.
- [9] G. Zhang, Q. Wu, M. Cui, and R. Zhang, "Securing UAV communications via trajectory optimization," in *Proc. IEEE Global Commun. Conf.*, Dec. 2017, pp. 1–6.
- [10] Y. Zhou, P. L. Yeoh, H. Chen, Y. Li, W. Hardjawana, and B. Vucetic, "Secrecy outage probability and jamming coverage of UAV-enabled friendly jammer," in *Proc. IEEE ICSPCS.*, Dec. 2017, pp. 1–6.
- [11] L. An, Q. Wu, and R. Zhang, "UAV-enabled cooperative jamming for improving secrecy of ground wiretap channel," *IEEE Wireless Commun. Lett.*, Aug. 2018.
- [12] Y. Zhou, P. L. Yeoh, H. Chen, Y. Li, R. Schober, L. Zhuo, and B. Vucetic, "Improving physical layer security via a UAV friendly jammer for unknown eavesdropper location," *IEEE Trans. Veh. Technol.*, vol. 67, no. 11, pp. 11 280–11 284, Nov. 2018.
- [13] X. Zhou, Q. Wu, S. Yan, F. Shu, and J. Li, "UAV-enabled secure communications: Joint trajectory and transmit power optimization," *IEEE Trans. Veh. Technol.*, vol. 68, no. 4, pp. 4069–4073, Apr. 2019.
- [14] Y. Cai, Z. Wei, R. Li, D. W. K. Ng, and J. Yuan, "Joint trajectory and resource allocation design for energy-efficient secure UAV communication systems," *IEEE Trans. Commun.*, vol. 68, no. 7, pp. 4536–4553, Jul. 2020.

- [15] B. A. Bash, D. Goeckel, D. Towsley, and S. Guha, "Hiding information in noise: Fundamental limits of covert wireless communication," *IEEE Commun. Mag.*, vol. 53, no. 12, pp. 26–31, Dec. 2015.
- [16] Z. Liu, J. Liu, Y. Zeng, and J. Ma, "Covert wireless communications in iot systems: Hiding information in interference," *IEEE Wireless Commun. Mag.*, vol. 25, no. 6, pp. 46–52, Dec. 2018.
- [17] S. Yan, X. Zhou, J. Hu, and S. V. Hanly, "Low probability of detection communication: Opportunities and challenges," *IEEE Wireless Commun. Mag.*, vol. 26, no. 5, pp. 19–25, Oct. 2019.
- [18] B. Bash, D. Goeckel, and D. Towsley, "Limits of reliable communication with low probability of detection on AWGN channels," *IEEE J. Sel. Areas Commun.*, vol. 31, no. 9, pp. 1921–1930, Sep. 2013.
- [19] B. He, S. Yan, X. Zhou, and V. Lau, "On covert communication with noise uncertainty," *IEEE Commun. Lett.*, vol. 21, no. 4, pp. 941–944, Apr. 2017.
- [20] T. V. Sobers, B. A. Bash, S. Guha, D. Towsley, and D. Goeckel, "Covert communication in the presence of an uninformed jammer," *IEEE Wireless Commun.*, vol. 16, no. 9, pp. 6193–6206, Sep. 2017.
- [21] J. Hu, S. Yan, X. Zhou, F. Shu, J. Li, and J. Wang, "Covert communication achieved by a greedy relay in wireless networks," *IEEE Trans. Wireless Commun.*, vol. 17, no. 7, pp. 4766–4779, Jul. 2018.
- [22] J. Wang, W. Tang, Q. Zhu, X. Li, H. Rao, and S. Li, "Covert communication with the help of relay and channel uncertainty," *IEEE Wireless Commun. Lett.*, vol. 8, no. 1, pp. 317–320, Feb. 2019.
- [23] X. Liao, J. Si, J. Shi, Z. Li, and H. Ding, "Generative adversarial network assisted power allocation for cooperative cognitive covert communication system," *IEEE Commun. Lett.*, vol. 24, no. 7, pp. 1463–1467, Jul. 2020.
- [24] K. Shahzad, X. Zhou, S. Yan, J. Hu, F. Shu, and J. Li, "Achieving covert wireless communications using a full-duplex receiver," *IEEE Trans. Wireless Commun.*, vol. 17, no. 12, pp. 8517–8530, Dec. 2018.
- [25] F. Shu, T. Xu, J. Hu, and S. Yan, "Delay-constrained covert communications with a full-duplex receiver," *IEEE Wireless Commun. Lett.*, vol. 8, no. 3, pp. 813–816, Jun. 2019.
- [26] T.-X. Zheng, H.-M. Wang, D. W. K. Ng, and J. Yuan, "Multi-antenna covert communications in random wireless networks," *IEEE Trans. Wireless Commun.*, vol. 18, no. 3, pp. 1974–1987, Mar. 2019.
- [27] X. Lu, W. Yang, Y. Cai, and X. Guan, "Proactive eavesdropping via covert pilot spoofing attack in multi-antenna systems," *IEEE Access*, vol. 7, pp. 151 295–151 306, Oct. 2019.
- [28] X. Zhou, S. Yan, J. Hu, J. Sun, and F. Shu, "Joint optimization of a UAV's trajectory and transmit power for covert communications," *IEEE Trans. Signal Process.*, vol. 67, no. 16, pp. 4276–4290, Aug. 2019.
- [29] H. Wang, Y. Zhang, X. Zhang, and Z. Li, "Secrecy and covert communications against UAV surveillance via multi-hop networks," *IEEE Trans. Commun.*, vol. 68, no. 1, pp. 389–401, Jan. 2020.
- [30] L. Xie, J. Xu, and Y. Zeng, "Common throughput maximization for UAV-enabled interference channel with wireless powered communications," *IEEE Trans. Commun.*, vol. 68, no. 5, pp. 3197–3212, May 2020.
- [31] S. Yan, B. He, X. Zhou, Y. Cong, and A. L. Swindlehurst, "Delay-intolerant covert communications with either fixed or random transmit power," *IEEE Trans. Inf. Forensics Security*, vol. 14, no. 1, pp. 129–140, Jan. 2019.
- [32] S. Yan, Y. Cong, S. Hanly, and X. Zhou, "Gaussian signalling for covert communications," *IEEE Trans. Wireless Commun.*, vol. 18, no. 7, pp. 3542–3553, Jul. 2019.
- [33] X. Sun, S. Yan, N. Yang, Z. Ding, C. Shen, and Z. Zhong, "Short-packet downlink transmission with non-orthogonal multiple access," *IEEE Trans. Wireless Commun.*, vol. 17, no. 7, pp. 4550–4564, Jul. 2018.